Cancer Science
Japanese Cancer Association JCA
Open Access

Angiotensin II subtype 1a receptor signaling in resident hepatic macrophages induces liver metastasis formation

Yuki Shimizu,[1,2] Hideki Amano,[1] Yoshiya Ito,[3] Tomohiro Betto,[1,2] Sakiko Yamane,[1,2] Tomoyoshi Inoue,[1,2] Nobuyuki Nishizawa,[1,3] Yoshio Matsui,[1] Mariko Kamata,[4] Masaki Nakamura,[5] Hidero Kitasato,[5] Wasaburo Koizumi[2] and Masataka Majima[1]

Departments of [1]Pharmacology; [2]Gastroenteology; [3]Surgery; [4]Nephrology, Kitasato University School of Medicine, Kanagawa; [5]Department of Microbiology, Kitasato University School of Allied Health Sciences, Kanagawa, Japan

Key words

Angiotensin, AT1a, colorectal cancer, Kupffer cell, liver metastasis

Correspondence

Hideki Amano, Department of Pharmacology, Kitasato University School of Medicine, 1-15-1 Kitasato, Minami-ku, Sagamihara, Kanagawa 252-0374, Japan.
Tel: +81-42-778-9164;
E-mail: hideki@kitasato-u.ac.jp

Funding Information

This research is supported by research grants 16K10688, 26462132, 23592073, and by a High-Tech Research Center grant from the Japanese Ministry of Education, Culture, Sports, Science, and Technology.

Received January 3, 2017; Revised June 20, 2017; Accepted June 25, 2017

Cancer Sci **108** (2017) 1757–1768

doi: 10.1111/cas.13306

Liver metastases from colorectal cancer (CRC) are a clinically significant problem. The renin–angiotensin system is involved in tumor growth and metastases. This study was designed to evaluate the role of angiotensin II subtype receptor 1a (AT1a) in the formation of liver metastasis in CRC. A model of liver metastasis was developed by intrasplenic injection of mouse colon cancer (CMT-93) into AT1a knockout mice (AT1aKO) and wild-type (C57BL/6) mice (WT). Compared with WT mice, the liver weight and liver metastatic rate were significantly lower in AT1aKO. The mRNA levels of CD31, transforming growth factor- β1 (TGF-β1), and F4/80 were suppressed in AT1aKO compared with WT. Double immunofluorescence analysis showed that the number of accumulated F4/80$^+$ cells expressing TGF-β1 in metastatic areas was higher in WT than in AT1aKO. The AT1aKO bone marrow (BM) (AT1aKO-BM)→WT showed suppressed formation of liver metastasis compared with WT-BM→WT. However, the formation of metastasis was further suppressed in WT-BM→AT1aKO compared with AT1aKO-BM→WT. In addition, accumulated F4/80$^+$ cells in the liver metastasis were not BM-derived F4/80$^+$ cells, but mainly resident hepatic F4/80$^+$ cells, and these resident hepatic F4/80$^+$ cells were positive for TGF-β1. Angiotensin II enhanced TGF-β1 expression in Kupffer cells. Treatment of WT with clodronate liposomes suppressed liver metastasis by diminishing TGF-β1$^+$F4/80$^+$ cells accumulation. The formation of liver metastasis correlated with collagen deposition in the metastatic area, which was dependent on AT1a signaling. These results suggested that resident hepatic macrophages induced liver metastasis formation by induction of TGF-β1 through AT1a signaling.

Colorectal cancer is a leading cause of cancer-related death in Japan that is associated with changes in lifestyle toward a Western diet.[1] Approximately 20% of patients with a diagnosis of CRC already have metastasis.[2] Liver metastasis is a common complication of CRC that has an impact on outcomes. The mechanisms of early metastasis formation remain unclear.

Resident and tumor-infiltrating cells form tumor microenvironments that have an important role in cancer initiation and progression.[3] These cells regulate the release of pro-inflammatory cytokines, chemokines, and pro-angiogenic factors.[4,5] Transforming growth factor-β1 is one of the major cytokines that induces phenotypic changes such as EMT of tumor cells, thereby facilitating their extravasation and dissemination to distant sites during metastasis.[6] Transforming growth factor-β1 is also known to be a promoter of tumor progression and profibrotic agent associated with the ability of EMT activator.[6]

The RAS plays an important role in the cardiovascular system and regulation of blood pressure.[7] Angiotensin II is converted to mediator Ang 1-8 by ACE.[8] The activation of Ang II has been shown to stimulate the expression of VEGF, SDF-1, and TGF-β1.[9,10] Angiotensin II is known to be mediated by seven transmembrane receptors, and two major subtypes have been identified, AT1 and AT2.[11] AT1 consists of two isoforms, AT1a and AT1b.[11] Previous studies showed that the genetic depletion of AT1a inhibits tumor cell growth.[12] We have also reported that the AT1 receptor antagonist TCV-116 or the genetic depletion of AT1a suppresses tumor growth and lung metastasis formation.[9] Previous studies have reported that the RAS inhibits growth of CRC liver metastasis in the regenerating liver.[13–15] The expressions of AT1 receptor in KCs and macrophages are increased in metastatic liver.[16] Blockade of AT1 receptor inhibits liver metastasis.[16] However, the precise mechanism of the contributions of AT1a receptor signaling to liver metastasis remains to be clarified. A recent study showed that uptake of tumor cell-derived exosomes by KCs induces TGF-β1 secretion and formation of a premetastatic niche.[17] These findings led us to hypothesize that the development of liver metastasis is facilitated by TGF-

β1 secreted from KCs through AT1a signaling. The present study was thus designed to investigate the role of AT1a signaling in liver metastasis and to explore the underlying mechanisms of metastasis regulated by AT1a signaling.

Materials and Methods

Animals. Male C57BL/6 mice, 6–8 weeks old and weighing 20–25 g, were obtained from the CLEA Japan Shizuoka Laboratory Animal Center (Fuji, Japan). AT1a knockout mice (AT1aKO) with a C57BL/6 hybrid background were generated by our research group. The mice were kept continuously on a 12:12-h light:dark cycle. All experiments were carried out in accordance with the guidelines for animal experiments of Kitasato University School of Medicine (Kanagawa, Japan).

Liver metastasis model. Mice were anesthetized by i.p. injection of pentobarbital sodium (50 mg/kg) throughout the experiments. The adequacy of anesthesia was monitored on the basis of disappearance of the pedal withdrawal reflex. The hair was shaved from the left flank, and the skin was rubbed with ethanol pads. A 0.5-cm incision was made in the left flank adjacent to the spleen, as described previously.[18] CMT-93 (CCL-223; ATCC, Manassas, VA, USA), a murine colorectal cancer cell line, was maintained in DMEM (Sigma, Tokyo, Japan) and RPMI-1640 medium (Sigma), containing 10% FBS. These cancer cells (2.0×10^6) in 200 μL PBS were slowly injected into the spleen of WT and AT1aKO using a 27-G needle. Five minutes after the injection, the spleen was removed, and the wound was closed with surgical clips. Two weeks after injection of CMT-93 cells, the mice were killed with an i.p. overdose of pentobarbital sodium (100 mg/kg). Liver metastases were identified macroscopically. The rate of hepatic metastases was expressed by dividing the number of mice with hepatic metastases by the total number of mice. The total numbers in WT and AT1a KO were 20, respectively. The livers were resected and weighed. Sections (4-μm thick) were prepared from paraffin-embedded tissue and stained with H&E. Images of H&E-stained sections were captured under a fluorescence microscope (Biozero BZ-9000 Series; Keyence, Osaka, Japan). The area of liver metastasis was measured using ImageJ software (Bethesda, MD, USA).

Real-time RT-PCR analysis. Transcripts encoding AT1a-R, AT1b-R, AT2-R, F4/80, TGF-β1, SDF-1 (CXCL12), VEGF-A, CD31, MCP-1 (CCL2), Col1a1, and GAPDH were quantified by real-time PCR analysis. Total RNA was extracted from liver tissues with TRIzol reagent (Gibco-BRL; Life Technologies, Rockville, MD, USA) and single-stranded cDNA was generated from 1 μg total RNA by RT with ReverTra Ace (Toyobo, New York, NY, USA). Quantitative PCR was carried out with SYBR Premix Ex Taq II (Takara Bio, Shiga, Japan). The real-time PCR primers were designed using Primer 3 software (http://primer3.sourceforge.net/) based on data from GenBank. The DNA sequences of mouse primers used for real-time PCR are described in Table 1. Data were normalized to the level of GAPDH in each sample.

Immunohistochemical analysis. Liver tissue was immediately fixed in 10% neutral buffered paraformaldehyde. After fixation, the tissue was dehydrated in a graded ethanol series and then embedded in paraffin. Each section (4 μm) of the paraffin-embedded tissue was mounted on a glass slide and either stained with H&E or processed for immunohistochemistry. For the latter, sections were activated using Histo VT One (Nacalai Tesque, Yokohama, Japan) and then incubated overnight at 4°C with one of the following primary antibodies: (a) anti-mouse F4/80 antibody (1:200, rat monoclonal, sc52664; Santa Cruz Biotechnology, Dallas, TX, USA); (b) anti-mouse TGF-β1 antibody (1:200, rabbit polyclonal, ab92486; Abcam, Cambridge, UK); (c) anti-mouse GFP antibody (1:200, rabbit polyclonal, ab290; Abcam); (d) anti-mouse Ang II type 1A receptor antibody (1:100, rabbit polyclonal, bs-2132R; Bioss, Boston, MA, USA); (e) anti-mouse desmin antibody (1:100, goat polyclonal, ab80503; Abcam); (f) anti-mouse type I collagen antibody (1:100, rabbit polyclonal, ab21286; Abcam); or (g) anti-mouse CD31 antibody (1:200, rabbit polyclonal, ab28364; Abcam). For primary antibodies (a–f), after washing in PBS, the sections were incubated for 2 h at room temperature with Alexa Fluor 488-conjugated donkey anti-rabbit IgG (Molecular Probes), Alexa Fluor 594-conjugated donkey anti-rat IgG (Molecular Probes, Eugene, OR, USA), and Alexa Fluor 594-conjugated donkey anti-goat IgG (Molecular Probes). For primary antibodies (f, g), after immersion in a 3% solution of hydrogen peroxide (H_2O_2) for 30 min, the sections were incubated for 30 min at room temperature with N-Histofine Simple Stain Mouse MAX PO (Nichirei Bioscience, Tokyo, Japan) and were immersed in 0.02% 3,3′-diaminobenzine and 0.3% nickel ammonium sulfate in 50 mM Tris-HCl buffer (pH 7.4) containing 0.005% H_2O_2 for 3 min. Images were captured with a light microscope and a fluorescence microscope (Biozero BZ-9000 Series; Keyence). For primary antibodies (a–e), the numbers of positive cells in metastases in the whole fields (×200 magnification) were counted. For primary antibody (f), the positive area in the whole fields (×200 magnification) was calculated with the use of ImageJ image analysis software.

Cell culture. The KUP5 KC line[19] was seeded on 12-well chamber glass slides (354 118; Corning, Corning, NY, USA) at a density of 1×10^5 cells/well with the growth medium. Three different concentrations of Ang II (0.001, 0.1, and 10 μM) were added to serum-free media for 6 and 12 h.

Green fluorescent protein BM transplantation. For the BM transplantation experiments, transgenic mice expressing GFP against a C57BL/6 background (a gift from Dr. M. Okabe, Genome Information Research Center, Osaka University, Osaka, Japan) were used to confirm BM chimerism. AT1aKO

Table 1. DNA sequences of mouse primers used for real-time RT-PCR

GAPDH	Sense	5′-ACATCAAGAAGGTGGTGAAGC-3′
	Antisense	5′-AAGGTGGAAGAGTGGGAGTTG-3′
AT1a-R	Sense	5′-GCATCATCTTTGTGGTGGG-3′
	Antisense	5′-ATCAGCACATCCAGGAATG-3′
AT1b-R	Sense	5′-GCATCATCTTTGTGGTGGG-3′
	Antisense	5′-ATGAGCACATCCAGAAAAC-3′
AT2-R	Sense	5′-ATGCTCAGTGGTCTGCTGG-3′
	Antisense	5′-AACACAGCTGTTGGTGAATCC-3′
F4/80	Sense	5′-TATCTTTTCCTCGCCTGCTTC-3′
	Antisense	5′-CACCACCTTCAGGTTTCTCAC-3′
TGF-β	Sense	5′-AACAATTCCTGGCGTTACCTT-3′
	Antisense	5′-TGTATTCCGTCTCCTTGGTTC-3′
SDF-1	Sense	5′-GCATCAGTGACGGTAAACCAG-3′
	Antisense	5′-GCACAGTTTGGAGTGTTGAGG-3′
VEGF-A	Sense	5′-GAGAGAGGCCGAAGTCCTTT-3′
	Antisense	5′-TTGGAAC-CGGCATCTTTATC-3′
CD31	Sense	5′-ACTTCTGAACTCCAACAGCGA-3′
	Antisense	5′-CCATGTTCTGGGGGTCTTTAT-3′
MCP-1	Sense	5′-CCCAATGAGTAGGCTGGAGAG-3′
	Antisense	5′-GTCTGGACCCATTCCTTCTTG-3′
Col1a1	Sense	5′-AGGCATAAAGGGTCATCGTG-3′
	Antisense	5′-GACCGTTGAGTCCGTCTTTG-3′

and GFP$^+$ mice were crossed to obtain GFP$^+$ AT1aKO. Bone marrow transplantation experiments were carried out as described previously.[20] In brief, donor BM was obtained by flushing the cavities of AT1aKO and WT/GFP transgenic mice with PBS. The flushed BM cells were dispersed and resuspended in PBS at a density of 1.0×10^6 cells/100 μL. Both WT and AT1aKO were lethally irradiated with 10 Gy using an MBR-1505 R X-ray irradiator (Hitachi Medico, Tokyo, Japan) equipped with a filter (copper, 0.5 mm; aluminum, 2 mm). The cumulative radiation dose was monitored. The BM mononuclear cells of GFP mice (2.0×10^6 cells/200 μL) were transplanted into irradiated WT and AT1aKO through the tail vein. After 8 weeks, blood was collected and analyzed by FACS. Mice in which more than 90% of peripheral leukocytes were GFP-positive were used in the experiments.

Measurement of protein levels of type I collagen. Protein levels of type I collagen in the liver at day 0 and day 14 after injecting cancer cells were measured using a specific ELISA kit (Mouse Type I collagen detection kit, 6012; Chondrex, Redmond, WA, USA).

Macrophage depletion model. To deplete KCs, mice were injected i.v. with 200 μL clodronate liposomes (F70101C-N; FormuMax Scientific, Palo Alto, CA, USA) or control liposomes (F70101-N) 2 days before cancer cell injection into the spleen.

Statistical analysis. Data are expressed as means ± SD. All statistical analyses were undertaken using GraphPad Prism software, version 5.01 (GraphPad Software, La Jolla, CA, USA). Student's *t*-test or the Mann–Whitney *U*-test were used for comparisons between two experimental groups with or without normal distribution, respectively. Comparisons between multiple groups were carried out using one-way ANOVA. The results of survival experiments were analyzed using log–rank tests and are presented as Kaplan–Meier survival curves. *P*-values <0.05 were considered to indicate statistical significance.

Results

AT1a expression rises on liver metastasis formation. We determined the expression of AT receptors in the metastatic livers from WT (C57BL/6) mice. Compared with PBS injection, the expression of AT1a in the metastatic liver was enhanced after injection of CMT-93 cells, whereas there were no significant differences in the expression of AT1b ($P = 0.057$) or AT2 ($P = 0.114$; Fig. 1a). These results suggested that AT1a signaling is related to liver metastasis formation.

AT1a-deficient mice suppress liver metastasis formation. To examine the effect of endogenous AT1a signaling on liver metastasis formation, we compared the liver weight and the rate of metastasis between AT1aKO and WT (Fig. 1b,c). Compared with WT, the liver weight (WT 1.32 ± 0.04 g *vs* AT1aKO 1.03 ± 0.01 g; $P < 0.05$; Fig. 1b) and rate of metastasis (WT 87.5 ± 8.5% *vs* AT1aKO 17.1 ± 5.7%; $P < 0.05$; Fig. 1c) were significantly suppressed in AT1aKO. The colon cancer cell line CMT-93 substantially formed liver metastases in WT mice, whereas liver metastasis formation was less in AT1aKO mice (Fig. 1d,e). We also confirmed that AT1aKO mice injected with another colon cancer cell line, Colon 38, significantly suppressed liver metastasis formation (Fig. S1).

The metastatic areas in the liver in macro (WT 2.64 ± 0.33 cm^2 *vs* AT1aKO 0.07 ± 0.07 cm^2; Fig. 1f) and in micro (WT 1.60 ± 0.56 mm^2 *vs* AT1aKO 0.08 ± 0.03 mm^2; Fig. 1g) were significantly suppressed in AT1aKO compared with WT. Furthermore, 60 days after the injection of CMT-93 cells, the survival rate of WT was 30%, while that of AT1aKO was 90% (Fig. 1h). These results suggested that AT1a signaling facilitates not only liver metastasis formation but also serves as a prognostic factor for liver metastasis.

AT1a has been suggested to be expressed in KCs[16] and HSCs.[21] To further examine the cellular source of AT1a in liver metastatic areas, dual immunofluorescence was carried out 14 days after CMT-93 injection. Immunofluorescence double staining of liver sections of WT with antibodies against AT1a and F4/80 or desmin, a marker for HSCs,[22] indicated that AT1a was expressed mainly in KCs (F4/80-positive cells; Fig. S2a), and partly in HSCs (desmin-positive cells; Fig. S2b). These results suggest that AT1a is derived mainly from KCs, and partly from HSCs, during the progression of CRC liver metastasis.

Suppressed angiogenesis and macrophage markers in AT1a-deficient mice during liver metastasis formation. Tumor metastasis formation is related to angiogenesis.[23] Therefore, we investigated the expressions of CD31, VEGF-A, SDF-1, and TGF-β1 in the liver 14 days after CMT-93 injection. The expression of CD31 mRNA was significantly suppressed in AT1aKO compared with WT (Fig. 2a). In addition, immunohistochemical analysis of CD31 showed that more CD31-positive cells were located in metastatic areas in WT than in AT1aKO (Fig. 2b). Furthermore, we examined the expression of angiogenesis-stimulating factors, including VEGF-A, SDF-1, and TGF-β1. The expression of TGF-β1 in the liver was significantly lower in AT1aKO than in WT, but there were no significant differences in VEGF-A or SDF-1 expression between the two groups (Fig. 2c–e). It is commonly accepted that macrophages are related to liver metastasis formation.[24] Macrophages secrete angiogenesis-stimulating factors to regulate metastasis formation. We therefore examined the expression of macrophage markers by means of real-time PCR analysis. The mRNA levels of F4/80 in livers from AT1aKO were significantly suppressed compared with the levels in livers from WT (Fig. 2f). The mRNA levels of MCP-1 in AT1aKO were also reduced (Fig. 2g). These results suggested that AT1a signaling is involved in the recruitment of macrophages, which has an important role in tumor growth.

AT1a signaling accumulates F4/80$^+$ KCs expressing TGF-β1 into regions of metastasis. Kupffer cells are the resident macrophages of the liver and contribute to the metastatic process.[25,26] To elucidate the role of hepatic macrophages in liver metastasis, we determined the numbers of hepatic macrophages by immunofluorescence analysis. As shown in Figure 3(a), F4/80$^+$ cells markedly accumulated into the metastatic tumors in WT compared with AT1aKO. Infiltrated F4/80$^+$ cells in metastatic areas were significantly increased in WT (5019 ± 699 cells/mm^2) compared with AT1aKO (1870 ± 656 cells/mm^2; Fig. 3b). A previous study showed that TGF-β1 released from KCs induces tumor cell adhesion.[17] The number of TGF-β1$^+$ cells in WT (3655 ± 439 cells/mm^2) was larger than in AT1aKO (1291 ± 414 cells/mm^2; Fig. 3c). To investigate whether F4/80$^+$ KCs in metastatic tumors express TGF-β1, we carried out double immunofluorescent analysis against TGF-β1 and F4/80 (Fig. 3a). The expression of TGF-β1 was colocalized with F4/80$^+$ cells. Accumulation of F4/80$^+$TGF-β1$^+$ cells in the metastatic areas in WT (2962 ± 363 cells/mm^2) was enhanced compared with AT1aKO (1064 ± 333 cells/mm^2; Fig. 3d).

Angiotensin II enhances expression of TGF-β1 in KCs. To further focus on the expression of TGF-β1 from KCs, we

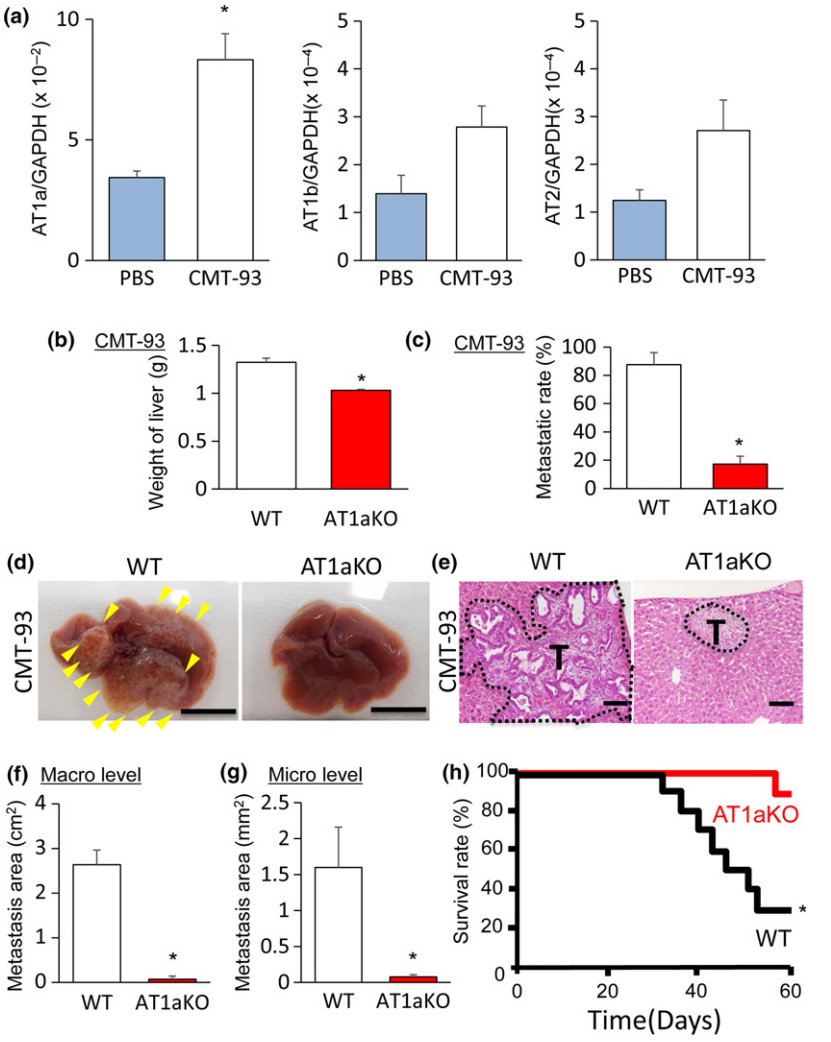

Fig. 1. Effect of AT1a signaling on liver metastasis formation. (a) Expressions of AT1a, AT1b, and AT2 receptor in metastatic livers 14 days after injection of CMT-93 mouse colon cancer cells. Data are expressed as the means ± SD of six mice per group. *$P < 0.05$ *versus* PBS-injected mice. (b,c). Effect of AT1a signaling on liver metastasis formation 14 days after injection of CMT-93 cells. The weight of liver metastasis (b) and the metastasis rate (c). Data are presented as the means ± SD of six mice per group. $P < 0.05$ *versus* WT. (d) Typical gross appearance of liver metastasis in WT and AT1aKO injected intrasplenically with CMT-93 cells. Arrows indicate metastatic colonization. Scale bar = 1 cm. (e) Typical appearance of H&E staining of metastatic livers from WT and AT1aKO after injection of CMT-93 cells. Metastatic area is delineated with the black dashed line. T, tumor. Scale bar = 100 μm. (f,g) Effects of AT1a signaling on colony formation in liver in macro (f) and micro (g) after injection of CMT-93 cells. Data are represented as the means ± SD of six mice per group. *$P < 0.05$ *versus* WT. (h) Mortality after injection of CMT-93 cells. The survival rate in WT was lower than that in AT1aKO. $n = 10$ per group. *$P < 0.05$ *versus* WT mice, Kaplan–Meier analysis.

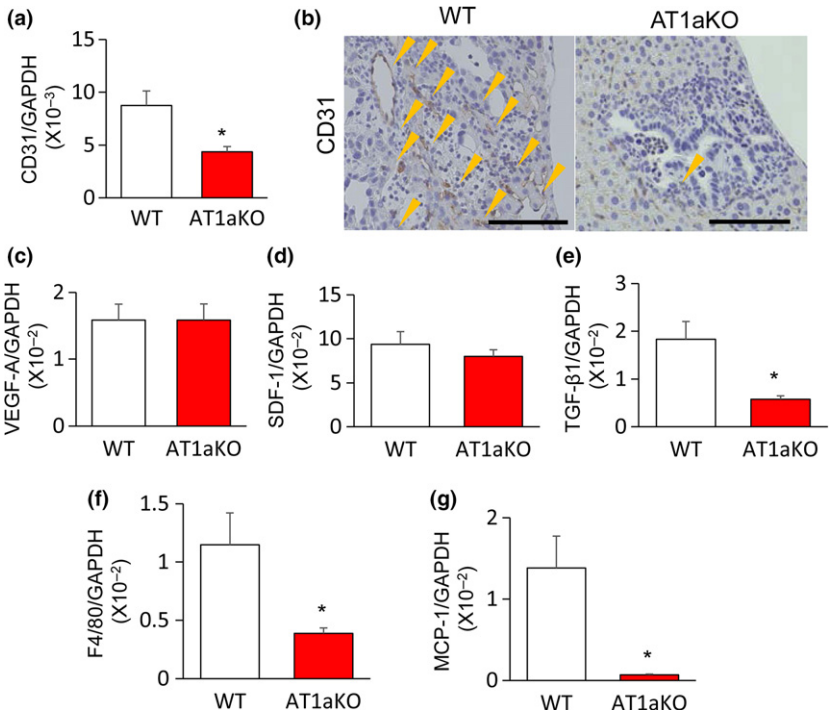

Fig. 2. AT1a signaling enhances the expression of angiogenic factor and macrophage marker in metastatic liver. (a,b) CD31 expression in the liver 14 days after injection of CMT-93 mouse colon cancer cells. Data are expressed as the means ± SD of six mice per group. *$P < 0.05$ *versus* WT. (a) mRNA level of CD31 was suppressed in AT1aKO mice. (b) Immunohistochemical staining of CD31 in metastatic areas from WT and AT1aKO mice. Scale bar = 100 μm. Arrows indicate CD31-positive cells. (c–e) Vascular endothelial growth factor A (VEGF-A) (c), stromal cell-derived factor-1 (SDF-1) (d), and transforming growth factor-β1 (TGF-β1) (e) mRNA expression in the liver 14 days after CMT-93 injection. Data are expressed as the means ± SD of six mice per group. *$P < 0.05$ *versus* WT. (f,g) F4/80 (f) and monocyte chemoattractant protein-1 (MCP-1) (g) mRNA expression in the liver 14 days after CMT-93 injection. Data are expressed as the means ± SD of six mice per group. *$P < 0.05$ *versus* WT.

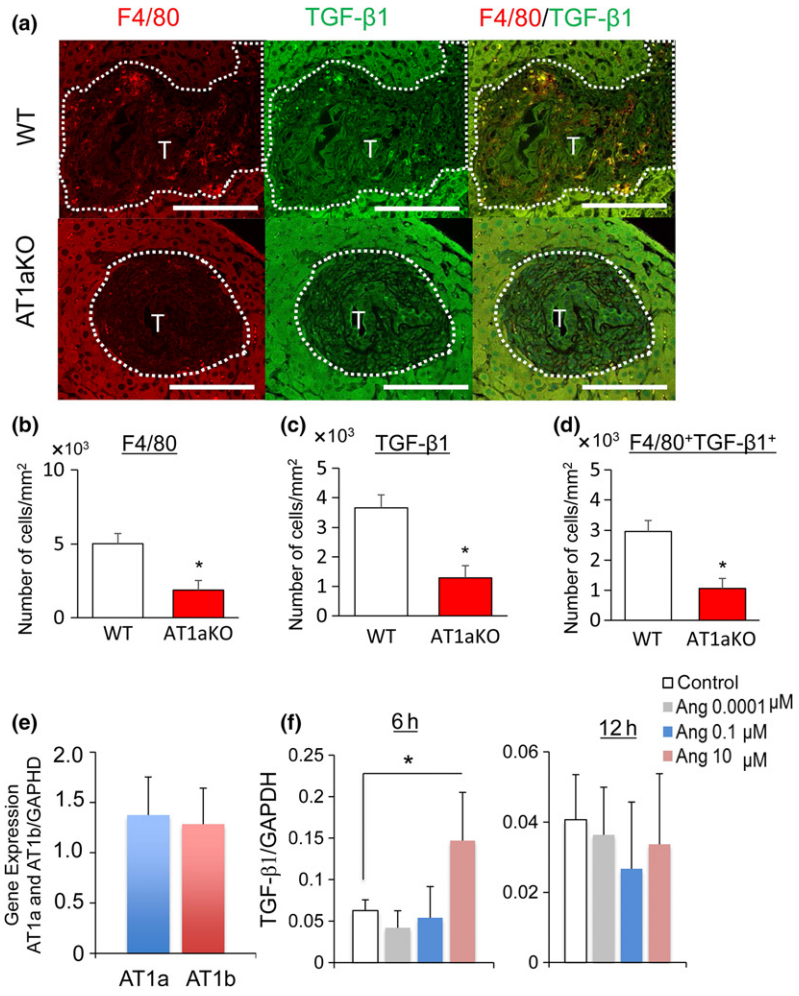

Fig. 3. Angiotensin II (Ang II)/AT1a axis enhances transforming growth factor-β1 (TGF-β1) expression in Kupffer cells. (a) Accumulation of F4/80$^+$ cells, TGF-β1$^+$ cells, and F4/80$^+$/TGF-β1$^+$ cells in metastatic areas from WT and AT1aKO mice on day 14. Double-staining of liver sections with antibodies against F4/80 (red) and TGF-β1 (green) in WT and AT1aKO mice. Expression of TGF-β1 was colocalized with F4/80$^+$ cells. Metastatic area is delineated with the white dashed line. T, tumor. Scale bar = 100 μm. (b–d) Numbers of F4/80$^+$ cells (b), TGF-β1$^+$ cells (c), and F4/80$^+$TGF-β1$^+$ cells (d) in metastatic areas from WT and AT1aKO mice. Data are expressed as the means ± SD of six mice per group. *P < 0.05. (e) Expression of AT1a and AT1b in KUP5 Kupffer cells. Data are expressed as the means ± SD of six mice per group. (f) Expression of TGF-β1 on KUP5 cells under stimulation with Ang II. Expression of TGF-β1 was enhanced 6 h after stimulation with Ang II compared with control. There was no significant difference at 12 h. Data are expressed as the means ± SD of six mice per group. *P < 0.05 *versus* control.

estimated the expression of TGF-β1 in mouse clonal KCs (KUP5) under Ang II stimulation. KUP5 expressed AT1 receptors, AT1a and AT1b (Fig. 3e). The expression of TGF-β1 was enhanced 6 h after stimulation with Ang II compared with the control (Fig. 3f). There was no significant difference in the expression of TGF-β1 at 12 h (Fig. 3f).

AT1a signaling in host cells is responsible for liver metastasis formation. To determine whether BM-derived macrophages affect liver metastasis formation, we transplanted GFP-expressing BM cells to irradiated mice: BM cells from GFP$^+$ WT or GFP$^+$ AT1aKO were transplanted→WT or AT1aKO. Eight weeks after BM transplantation, CMT-93 cells were intrasplenically implanted in chimeric mice (Fig. 4a). In AT1aKO-BM→WT, tumor area (1.97 ± 0.11 cm^2) was significantly suppressed compared with that in WT-BM→WT (2.94 ± 0.16 cm^2; Fig. 4b). Moreover, tumor area in WT-BM→AT1aKO (0.72 ± 0.15 cm^2) showed a significant increase compared with that in AT1aKO-BM→AT1aKO (0.17 ± 0.12 cm^2; Fig. 4b). These results suggested that AT1a signaling in BM cells is involved in liver metastasis. Interestingly, the tumor area in WT-BM→AT1aKO did not increase, but further decreased compared with that in AT1aKO-BM→WT. These results suggested that resident liver cells expressing AT1a rather than BM-derived cells expressing AT1a would induce metastatic formation.

Host-derived F4/80$^+$ cells participate in tumor metastasis formation. To further examine the contribution of BM-derived macrophages or host-derived macrophages to the formation of liver metastasis, immunofluorescence was carried out (Fig. 4c). The numbers of accumulated GFP$^+$ cells in AT1aKO-BM→WT (5917 ± 461 cells/mm^2), WT-BM→AT1aKO (6018 ± 622 cells/mm^2) and AT1aKO-BM→AT1aKO (5891 ± 825 cells/mm^2) had a tendency to be suppressed compared with those in WT-BM→WT (8269 ± 422 cells/mm^2; Fig. 5a). However, the difference did not reach statistical significance. This result suggested that AT1a signaling in BM cells did not make a significant contribution to the accumulation of BM-derived cells (GFP$^+$ cells) into metastatic areas.

The numbers of accumulated F4/80$^+$ cells in WT-BM→AT1aKO (3902 ± 451 cells/mm^2) were suppressed compared with WT-BM→WT (6172 ± 635 cells/mm^2; Fig. 5b). However, there were no significant differences in accumulated F4/80$^+$ cells between WT-BM→WT and AT1aKO-BM→WT. Similarly, the numbers of accumulated F4/80$^+$ cells in AT1aKO-BM→AT1aKO (2622 ± 409 cells/mm^2) were suppressed compared with AT1aKO-BM→WT (4754 ± 242 cells/mm^2; Fig. 5b). However, the numbers of F4/80$^+$ cells did not differ between AT1aKO-BM→WT and AT1aKO-BM→AT1aKO-BM. These results showed that hepatic resident cells expressing AT1a signaling, but not BM-derived cells, contributed to accumulation of F4/80$^+$ cells into liver metastatic lesions.

In order to examine whether F4/80$^+$ cells derive from BM or not, we counted the numbers of GFP$^+$F4/80$^+$ cells (Fig. 5c)

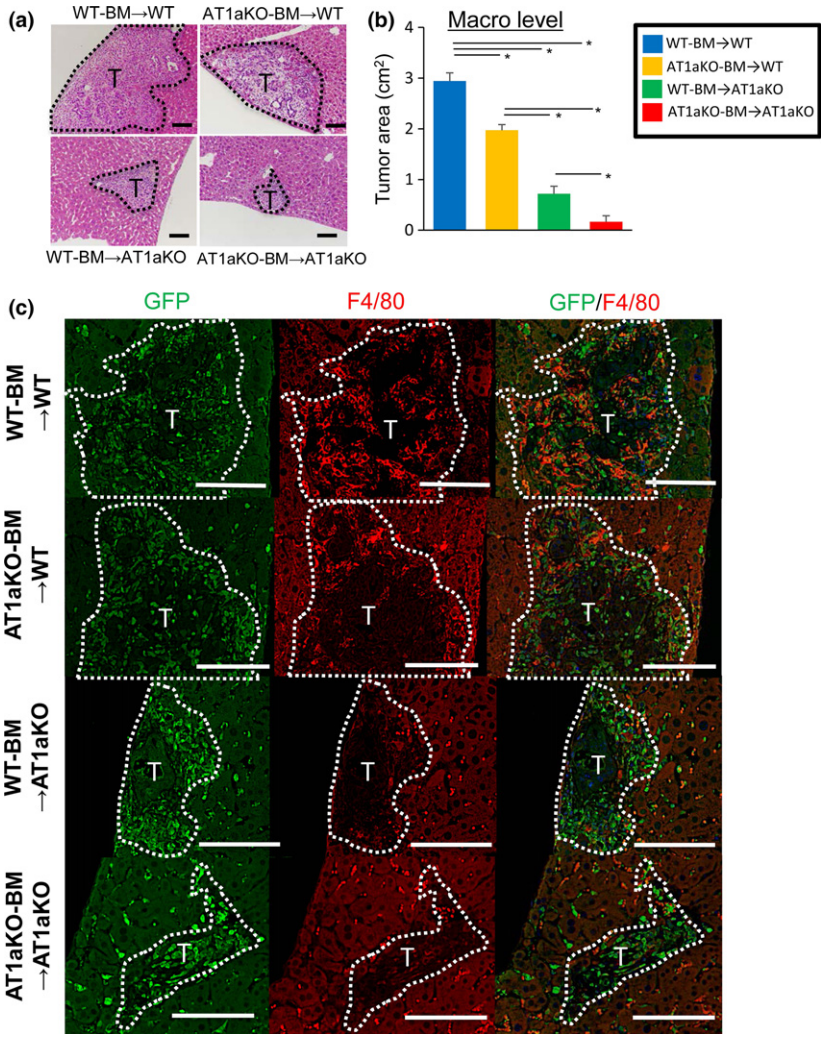

Fig. 4. Effects of bone marrow (BM) transplantation on liver metastasis. (a) Typical appearance of H&E staining of metastatic livers from chimeric mice 14 days after injection of CMT-93 mouse colon cancer cells. Metastatic area is delineated with the black dashed line. T, tumor. Scale bar = 100 μm. (b) Effect of BM transplantation on tumor area 14 days after CMT-93 injection. Metastatic tumor areas in AT1aKO-BM→WT and AT1aKO-BM→AT1aKO mice were suppressed compared with those in WT-BM→WT and WT-BM→AT1aKO mice, respectively. Data are expressed as the means ± SD of six mice per group. $*P < 0.05$ *versus* control. (c) Accumulation of $GFP^+F4/80^+$ cells in the metastatic area (delineated with white dashed line) on day 14. T, tumor. Scale bar = 100 μm.

and $GFP^-F4/80^+$ cells in metastatic areas (Fig. 5d). There were no significant differences in the numbers of $GFP^+F4/80^+$ cells among four groups (Fig. 5c). By contrast, the changes in numbers of $GFP^-F4/80^+$ cells in metastatic areas from each group were basically similar to those of $F4/80^+$ cells in each group (Fig. 5d).

The numbers of $GFP^+F4/80^+$ cells in WT-BM→WT were approximately 23% of the total numbers of $F4/80^+$ cells in WT-BM→WT, whereas the numbers of $GFP^-F4/80^+$ cells were approximately 77% of the total numbers of $F4/80^+$ cells (Fig. 5e). In addition, in another three groups, the percentages of $GFP^+F4/80^+$ cells were approximately 20%–30%, whereas those of $GFP^-F4/80^+$ cells were approximately 70%–80% (Fig. 5e). These results indicated that accumulated $F4/80^+$ cells in metastatic areas were mainly derived from resident hepatic macrophages (KCs) and partly from BM, and that resident KCs were mainly involved in tumor metastasis. These findings also suggested that AT1a signaling in resident KCs would contribute to liver metastasis formation.

$F4/80^+$ cells expressing TGF-β1 correlate with tumor metastasis formation. As indicated in Figure 3(a), we examined whether accumulated $F4/80^+$ cells expressed TGF-β1 in the BM transplantation model (Fig. 6a). $F4/80^+$ cells were also positive for TGF-β1 (Fig. 6a). The numbers of accumulated TGF-$β1^+$ cells in the metastatic livers from chimeric mice correlated with the numbers of accumulated $F4/80^+$ cells from respective chimeric mice (Fig. 6a,b). The total population of TGF-$β1^+F4/80^+$ cells in WT-BM→AT1aKO (2056 ± 171 cells/mm^2) was significantly reduced compared with that in WT-BM→WT (3268 ± 396 cells/mm^2; Fig. 6c). In addition, the total population of TGF-$β1^+F4/80^+$ cells in AT1aKO-BM→AT1aKO (1735 ± 277 cells/mm^2) had a tendency to be suppressed compared with that in AT1aKO-BM→WT (2233 ± 231 cells/mm^2; Fig. 6c). These results suggested that AT1a signaling accumulated host-derived TGF-$β1^+F4/80^+$KCs in metastatic areas.

AT1a signaling induces expression of type I collagen in metastatic areas. Because AT1a was expressed in HSCs (Fig. S2b), and type I collagen deposition produced by HSCs[27] is associated with an increased risk of liver metastasis,[28] we examined the cellular source of collagen deposition in metastatic areas. Double immunofluorescence revealed that the expression of type I collagen was colocalized with $desmin^+$ cells (Fig. S3a), but not $F4/80^+$ cells (Fig. S3b). Next, we determined the expression of type I collagen in metastatic areas 14 days after injection of CMT-93 cells in WT and AT1aKO. Immunohistochemical analysis showed that the expression of type I collagen in metastatic areas was diminished in AT1aKO (Fig. 7a). Quantitative analysis revealed that the total type I collagen-positive area in the liver from AT1aKO (0.05 ± 0.01 mm^2/

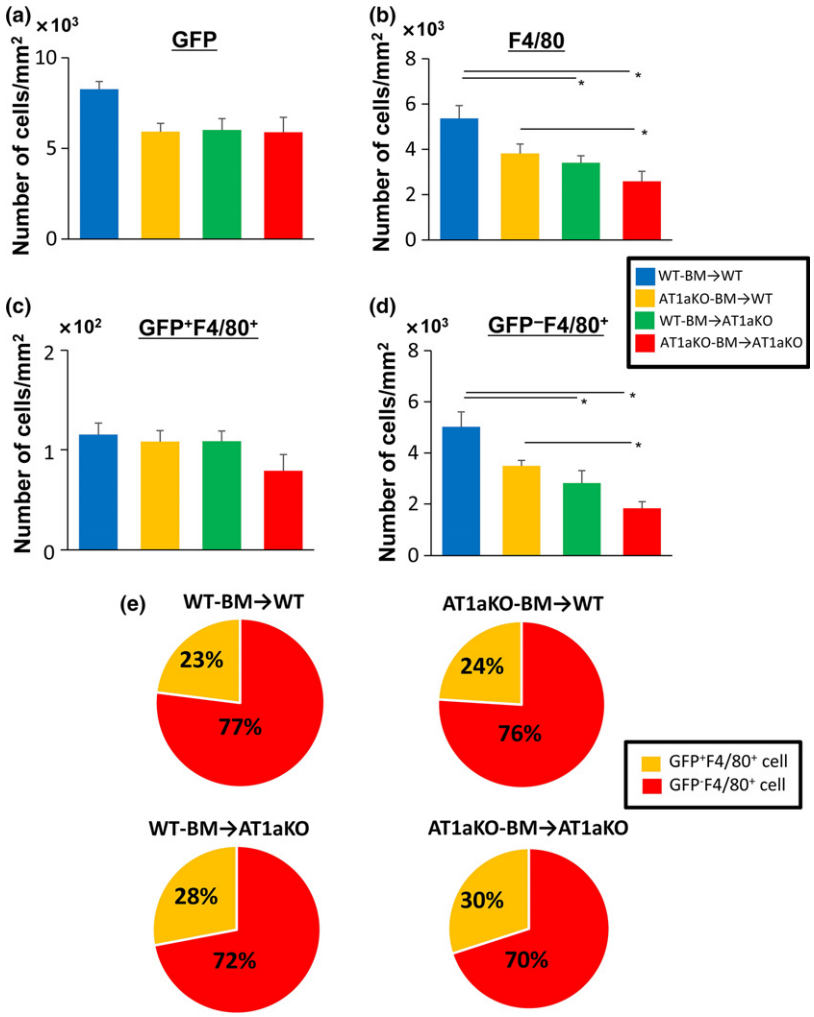

Fig. 5. Contribution of resident F4/80$^+$ Kupffer cells to liver metastasis formation. (a–d) Numbers of GFP$^+$ (a), F4/80$^+$ (b), GFP$^+$F4/80$^+$ cells (c), and GFP$^-$F4/80$^+$ cells (d) in metastatic areas. Data are expressed as the means ± SD of six mice per group. *$P < 0.05$. (e) Percentages of GFP$^+$F4/80$^+$ cells and GFP$^-$F4/80$^+$ cells in each group. BM, bone marrow.

mm^2) was suppressed compared with WT (0.19 ± 0.03 mm^2/mm^2; Fig. 7b). The mRNA expression of Col1a1 in AT1aKO was significantly reduced compared with that in WT (Fig. 7c). Moreover, the protein levels of type I collagen in the livers in AT1aKO (0.42 ± 0.02 μg/mL) was suppressed compared with those in WT (0.76 ± 0.13 μg/mL; Fig. 7d). These results suggested that HSCs produced type I collagen through AT1a signaling in liver metastatic areas. Bone marrow transplantation experiments showed that the area occupied by type I collagen-positive cells was significantly increased in WT-BM→WT (0.15 ± 0.02 mm^2/mm^2) compared with WT-BM→AT1aKO (0.08 ± 0.01 mm^2/mm^2). Similarly, those cells had a tendency to an increase in AT1aKO-BM→WT (0.09 ± 0.01 mm^2/mm^2) compared with AT1aKO-BM→AT1aKO (0.04 ± 0.01 mm^2/mm^2; Fig. 7e,f). These results suggested that the expression of type I collagen depended on AT1a signaling in host liver cells.

Infiltrated KCs contribute to liver metastasis formation. To further elucidate the role of KCs in liver metastasis formation, KCs from WT mice were deleted by injection of clodronate liposomes 2 days before injection of cancer cells. The metastasis area in WT with clodronate liposomes (1.15 ± 0.45 cm^2) was reduced compared with that in WT with control liposomes (3.30 ± 0.19 cm^2; Fig. 8a). The mRNA expression levels of F4/80, TGF-β1, Col1a1, and CD31 were significantly suppressed in WT with clodronate liposomes compared with WT with control liposomes (Fig. 8b–e). The numbers of TGF-β1$^+$ cells, F4/80$^+$ cells, and TGF-β1$^+$F4/80$^+$ cells were suppressed in clodronate liposome-treated WT (1267 ± 472, 1959 ± 596, and 970 ± 378 cells/mm^2, respectively) compared with controls (5205 ± 401, 6399 ± 520, and 4192 ± 402 cells/mm^2, respectively; Fig. 8f–i). The area occupied by type I collagen-positive cells was suppressed in clodronate liposome-treated mice (0.11 ± 0.02 mm^2/mm^2) compared with control liposome-treated mice (0.33 ± 0.04 mm^2/mm^2; Fig. 8j,k). These results suggested that the accumulation of KCs expressing TGF-β1 induces liver metastasis formation associated with production of type I collagen.

Discussion

The focus of this study was to elucidate the role of AT1a signaling in the metastatic progression of CRC in the liver. The genetic depletion of AT1a significantly suppressed liver metastasis. Enhanced mRNA expression of F4/80 and TGF-β1 in the liver metastatic area was associated with the accumulation of F4/80$^+$ cells expressing TGF-β1. Bone marrow transplantation experiments showed the presence of mainly host-derived F4/80$^+$ cells (KCs), but BM-derived F4/80$^+$ cells, to a lesser degree, participated in liver metastasis formation. These results suggested that AT1a signaling promotes liver metastasis formation by accumulated resident hepatic macrophages in association with TGF-β1.

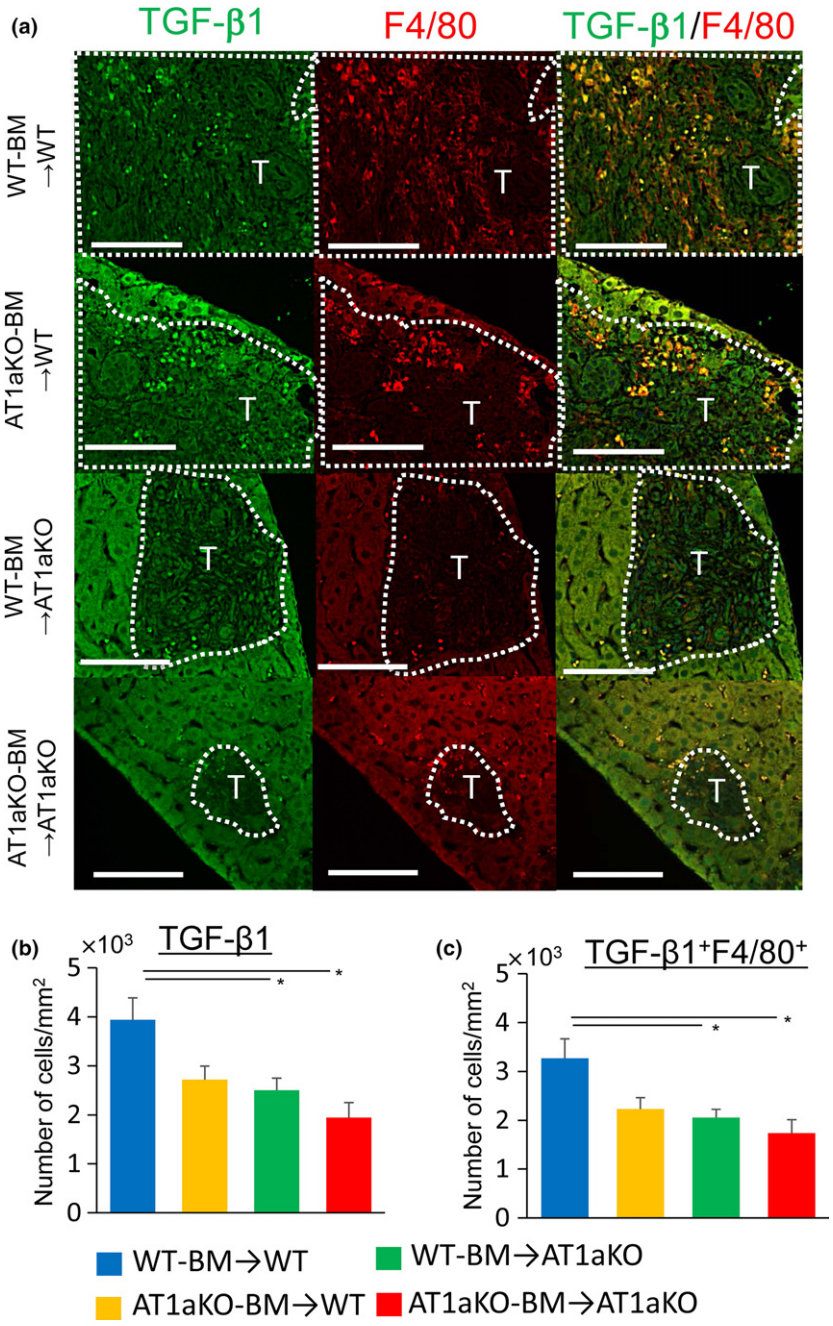

Fig. 6. Effect of AT1a signaling in bone marrow (BM) cells on accumulation of F4/80$^+$ cells expressing transforming growth factor-β1 (TGF-β1). (a) Accumulation of TGF-β1 $^+$F4/80$^+$ Kupffer cells in the metastatic areas (delineated with the white dashed line) on day 14. T, tumor. Scale bar = 100 μm. (b,c) Total numbers of TGF-β1$^+$ (b) and TGF-β1$^+$F4/80$^+$ Kupffer cells (c) in metastatic areas. Data are expressed as the means ± SD of six mice per group. *P < 0.05.

Angiotensin II is one of the major components of the RAS that is essential for blood pressure regulation and electrolyte balance.[6] Angiotensin II binds two receptors, AT1 and AT2. AT1 has two subtypes, receptor AT1a and AT1b.[11] Angiotensin II, one of the factors of the RAS, promotes tumor growth with expression of VEGF-A, angiopoietin 2, fibroblast growth factor, and platelet-derived growth factor.[3,4,29] The expression of AT1 is especially enhanced in cancer.[30–32] In fact, it is reported that ACE inhibitors and angiotensin II receptor blockers inhibit the risk of cancer and cancer-related death.[33] We have shown that AT1 signaling induces tumor growth and metastasis formation in a lung metastasis model.[9] Neo *et al.*[34] reported that treatment with ACE inhibitors suppressed angiogenesis in a mouse model of CRC liver metastasis. These findings led us to focus on the role of AT1a signaling in liver metastasis formation. To examine whether endogenous AT1a signaling has an effect on liver metastasis formation or not, we used AT1aKO. The present study showed suppression of liver metastasis formation in AT1aKO after injection of CMT-93 cells. We found that AT1a is expressed mainly in KCs during the progression of CRC liver metastasis, which is consistent with the findings by others.[16]

Liver metastasis formation is enhanced by angiogenesis-stimulating factors, including TGF-β1, VEGF-A, and SDF-1.[4,5] Transforming growth factor-β1 plays important roles in embryonic development, cell proliferation, differentiation, angiogenesis, and wound healing.[35,36] Furthermore, it is well known to be an immune and inflammation regulator. Upregulation of TGF-β1 induces EMT, a key step in processing metastasis formation, and this creates a microenvironment conducive to

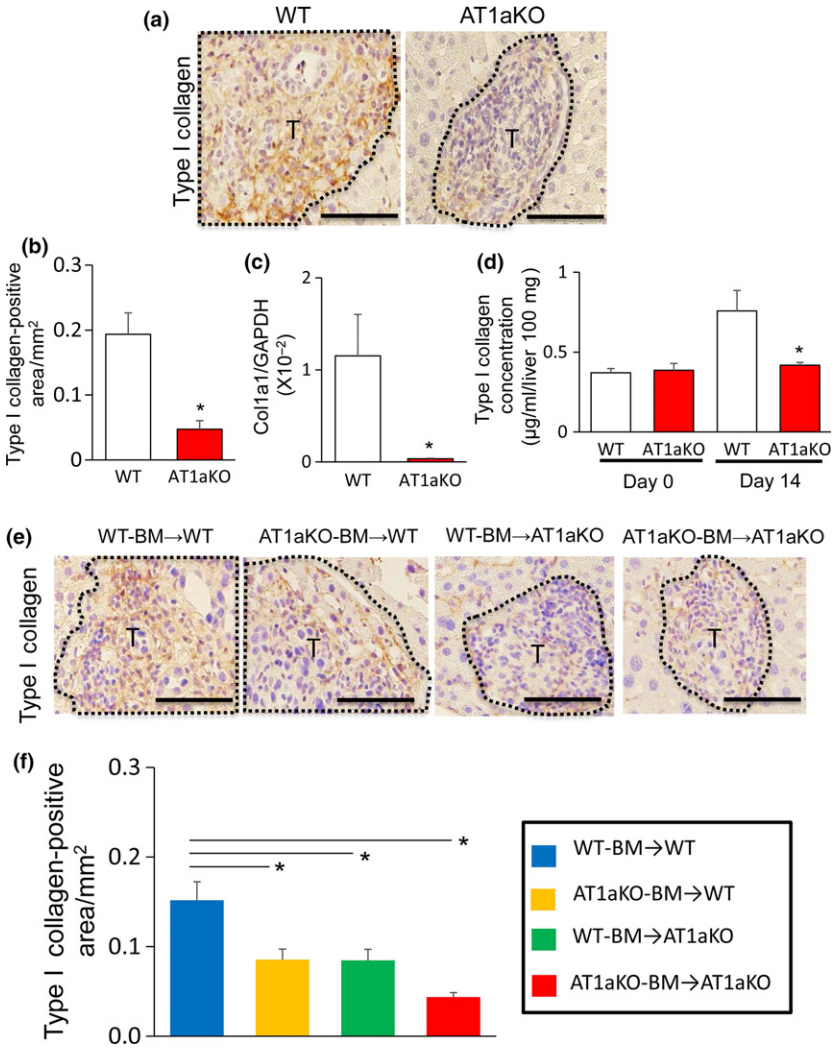

Fig. 7. Effect of AT1a signaling on type I collagen expression in metastatic areas. Immunohistochemical analysis of type I collagen in metastatic livers from WT and AT1aKO mice. Metastatic areas are delineated with the black dashed line. T, tumor. Scale bar = 100 μm. (a) Type I collagen-positive areas in metastatic livers from WT and AT1aKO mice. Data are expressed as the means ± SD of six mice per group. $*P < 0.05$. (b) Expression of collagen type I α1 (Col1a1) in metastatic livers from WT and AT1aKO mice. Data are expressed as the means ± SD of six mice per group. $*P < 0.05$. (c) Concentrations of type I collagen in metastatic livers from WT and AT1aKO mice at 0 and 14 days after CMT-93 injection. Data are expressed as the means ± SD of six mice per group. $*P < 0.05$. (d) Immunohistochemical staining of type I collagen in metastatic areas (delineated with black dashed line) after bone marrow (BM) transplantation. T, tumor. Scale bar = 100 μm. (e) Type I collagen-positive areas in metastatic livers from chimeric mice given transplants of BM from WT and AT1aKO. Data are expressed as the means ± SD of six mice per group. $*P < 0.05$.

infiltration of the target organ by cancer cells.[37] The present study showed that the expression of TGF-β1 in the metastatic liver was suppressed in AT1aKO compared with WT. This finding suggested that the expression of TGF-β1 in the metastatic liver was dependent on AT1a signaling. Taken together, AT1a signaling promotes liver metastasis with enhancement of TGF-β1.

The TGF-β1 signaling pathway is a key player in tumor development. Angiotensin II activates TGF-β1 signaling.[38] In the current study, we showed that F4/80+ KCs coexpressed TGF-β1 in metastatic areas and the expression of TGF-β1 depended on AT1a signaling. We also revealed that Ang II enhanced TGF-β1 expression in cultured KCs. Although these findings suggest that Ang II/AT1a activates the TGF-β1 signaling pathway, we further need to elucidate the relative importance of AT1a for activation of TGF-β1 signaling in a liver metastasis model.

Macrophages are characterized by high functional plasticity for forming tumor microenvironments that are associated with angiogenesis or facilitation of immune response.[39] Resident liver macrophages, KCs, play critical roles in development of microenvironments in primary cancer and liver metastasis formation.[40] Our present study showed that the expression of macrophage-related markers, including F4/80 and MCP-1, was enhanced in areas of metastasis. These results support the hypothesis that macrophages are related to metastasis formation.

Pancreatic cancer exosomes initiate premetastatic niche formation by KCs through TGF-β1 secretion.[17] Previous studies have shown that KCs express the RAS components ACE and AT1R. Wen *et al.*[16] reported that the RAS regulates KCs in CRC liver metastasis formation. In the present study, we showed that KUP5 cells, murine KCs, enhanced the expression of TGF-β1 under Ang II stimulation.

In this experiment, immunofluorescence against F4/80 was used to detect accumulated macrophages in the metastatic livers. Our results indicated that resident KCs had an important role in liver metastasis formation. We previously reported that AT1a signaling is important for the recruitment of BM cells to metastatic areas.[9] The present study showed that recruitment of GFP^+ cells infiltrated in liver metastasis was suppressed in AT1aKO-BM→WT compared with WT-BM→WT. Regardless of whether WT-BM or AT1aKO-BM was transplanted, the number of $GFP^+F4/80^+$ KCs was suppressed in AT1aKO. Interestingly, the same phenomenon was seen in the numbers of TGF-$\beta1^+F4/80^+$ KCs in WT-BM→WT and AT1aKO-BM→WT. Even after transplantation of WT-BM, the total population of $GFP^+F4/80^+$ KCs was not elevated. Moreover, the number of accumulated TGF-$\beta1^+F4/80^+$ KCs in the metastasis area was much higher than that of $GFP^+F4/80^+$ KCs in WT-BM→

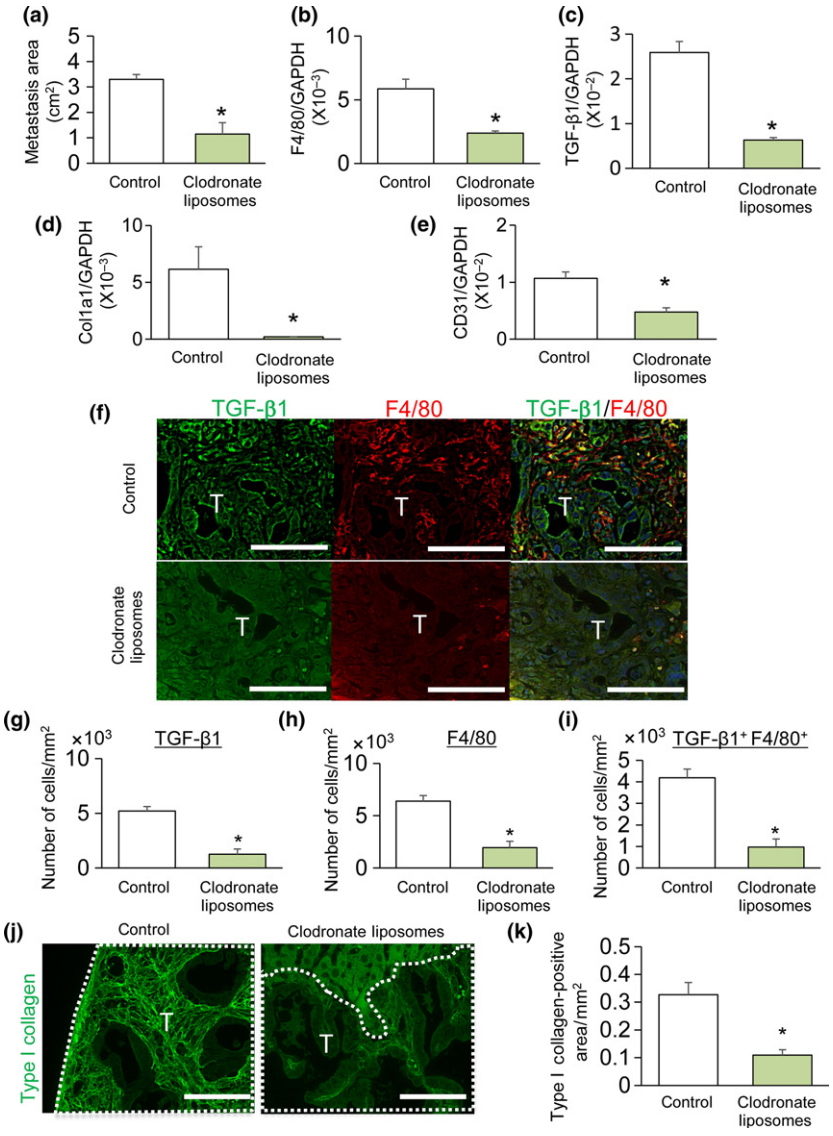

Fig. 8. Effects of macrophage deletion on liver metastasis formation. (a) Metastasis area in WT with control liposomes and clodronate liposomes 14 days after injection CMT-93 mouse colon cancer cells. Data are expressed as the means ± SD of four mice per group. **P* < 0.05 *versus* control liposomes. (b–e). F4/80 (b), transforming growth factor-β1 (TGF-β1) (c), collagen type I α1 (Col1a1) (d), and CD31 (e) mRNA expression in metastatic liver 14 days after CMT-93 injection. Data are expressed as the means ± SD of four mice per group. **P* < 0.05 *versus* control liposomes. (f) Accumulation of TGF-β1$^+$ cells, F4/80$^+$ cells, and TGF-β1$^+$/F4/80$^+$ cells in metastatic areas on day 14. Double-staining of liver sections with antibodies against TGF-β1 (green) and F4/80 (red). T, tumor. Scale bar = 100 μm. (g–i) Numbers of TGF-β1$^+$ cells (g), F4/80$^+$ cells (h), and TGF-β1$^+$ F4/80$^+$ cells (i) in metastatic areas from WT mice with control liposomes and clodronate liposomes. Data are expressed as the means ± SD of four mice per group. **P* < 0.05. (j) Representative images showing immunofluorescence staining for type I collagen in metastatic livers of WT mice with control liposomes and clodronate liposomes 14 days after CMT-93 injection. Metastatic area is delineated with the white dashed line. T, tumor. Scale bar = 100 μm. (k) Type I collagen-positive area in metastatic livers of WT mice with control liposomes and clodronate liposomes. Data are expressed as the means ± SD of four mice per group. **P* < 0.05.

WT. These results indicated that tissue resident TGF-β1$^+$F4/80$^+$ KCs play a role in metastasis formation through AT1a signaling, and that the number of TGF-β1$^+$F4/80$^+$ KCs correlated with liver metastasis formation.

Regarding the role of KCs in the formation of liver metastasis, conflicting results have been reported. Wen *et al.*[41] showed that KC depletion with gadolinium chloride before tumor induction was associated with an increased tumor burden in metastatic liver, suggesting that KCs show an antitumor effect. Kruse *et al.*[42] reported that KC depletion with clodronate liposomes before tumor induction led to a significant reduction of liver metastasis, which was consistent with our results. These suggest that KCs promote the formation of metastases in the liver. Despite divergent roles of KCs in liver metastasis, KC infiltration appears not to be the result of liver metastasis but the cause of initiation of liver metastasis. As the precise correlation between KCs and liver metastasis still remains unclear, further experiments are needed.

Tumor progression and fibrosis are pivotal aspects of malignant tumors. Several factors, including TGF-β1, VEGF-A, SDF-1, and Ang II, are regarded as candidate factors involved in cross-talk between tumor cells and stromal cells. As mentioned above, Ang II induces fibrosis in many organs. We previously reported that host-derived AT1a-positive cells, fibroblasts, induce tumor growth.[12] The present study suggested that TGF-β1 derived from resident KCs induced liver metastasis formation. We also showed that attenuated expression of host-derived TGF-β1 in AT1aKO was associated with suppressed metastasis formation.

In the early stage of metastasis, tumor cell invasion into the extra-sinusoidal space seems to recapitulate this tissue repair process: KCs trigger HSCs and liver sinusoidal endothelial cell activation. This was observed in experimental models and is also evidenced by the increased production of collagen in hepatic metastases in clinical specimens.[40] Okamoto *et al.*[43] showed that the Ang II/AT-1 axis induced tumor progression and fibrosis in intrahepatic cholangiosarcoma through an interaction with HSC. The present study indicated that the expression of type I collagen, a fibrosis marker, was also suppressed in AT1aKO. We showed that resident F4/80$^+$ KCs expressed TGF-β1 in metastatic tumor areas, in which type I collagen was significantly expressed. Transforming growth factor-β1 mediates fibrogenesis, including collagen deposition, by

induction of activated HSCs. Bone marrow transplantation experiments showed that AT1a signaling in host cells accumulated TGF-β1$^+$F4/80$^+$ KCs as well as type 1 collagen-productive cells. Further studies are needed to disclose the interaction between accumulated host-derived TGF-β1$^+$F4/80$^+$ KCs and fibrosis formation.

In conclusion, AT1a signaling in resident F4/80$^+$ KCs promotes liver metastasis formation by enhancing TGF-β1 expression. Highly selective AT1a antagonists may become a useful treatment for CRC.

Acknowledgments

We thank Michiko Ogino, Kyoko Yoshikawa, Mieko Hamano, and Osamu Katsumata for their technical assistance.

Disclosure Statement

The authors have no conflict of interest.

Abbreviations

ACE	angiotensin-converting enzyme
Ang	angiotensin
AT1aKO	AT1a knockout mice
BM	bone marrow
Col1a1	collagen type I α1
CRC	colorectal cancer
EMT	epithelial–mesenchymal transition
HSC	hepatic stellate cell
KC	Kupffer cell
MCP-1	monocyte chemoattractant protein-1
RAS	renin–angiotensin system
SDF-1	stromal cell-derived factor-1
TGF-β1	transforming growth factor-β1
VEGF	vascular endothelial growth factor

References

1 Kono S. Secular trend of colon cancer incidence and mortality in relation to fat and meat intake in Japan. *Eur J Cancer Prev* 2004; **13**: 127–32.
2 Fujimoto Y, Nakanishi Y, Sekine S *et al.* CD10 expression in colorectal carcinoma correlates with liver metastasis. *Dis Colon Rectum* 2005; **48**: 1839–89.
3 Itatani Y, Kawada K, Inamoto S *et al.* The role of chemokines in promoting colorectal cancer invasion/metastasis. *Int J Mol Sci* 2016 (Apr 28);**17**: pii: E643. https://doi.org/10.3390/ijms17050643.
4 Bianchi G, Borgonovo G, Pistoia V *et al.* Immunosuppressive cells and tumour microenvironment: focus on mesenchymal stem cells and myeloid derived suppressor cells. *Histol Histopathol* 2011; **26**: 941–51.
5 Ochiumi Tl, Kitadai Y, Tanaka S *et al.* Neuropilin-1 is involved in regulation of apoptosis and migration of human colon cancer. *Int J Oncol* 2006; **29**: 105–16.
6 Nalluri SM, O'Connor JW, Gomez EW. Cytoskeletal signaling in TGFβ-induced epithelial-mesenchymal transition. *Cytoskeleton (Hoboken).* 2015; **72**: 557–69.
7 Ibrahim J, Hughes AD, Sever PS. Action of angiotensin II on DNA synthesis by human saphenous vein in organ culture. *Hypertension* 2000; **36**: 917–21.
8 Calò LA, Schiavo S, Davis PA *et al.* ACE2 and angiotensin 1-7 are increased in a human model of cardiovascular hyporeactivity: pathophysiological implications. *J Nephrol.* 2010; **23**: 472–7.
9 Amano H, Ito Y, Ogawa F *et al.* Angiotensin II type 1A receptor signaling facilitates tumor metastasis formation through P-selectin-mediated interaction of tumor cells with platelets and endothelial cells. *Am J Pathol* 2013; **182**: 553–64.
10 Macconi D, Remuzzi G, Benigni A. Key fibrogenic mediators: old players. Renin-angiotensin system. *Kidney Int Suppl* 2011; **2014**(4): 58–64.
11 Kim S, Iwao H. Molecular and cellular mechanisms of angiotensin II-mediated cardiovascular and renal diseases. *Pharmacol Rev* 2000; **52**: 11–34.
12 Fujita M, Hayashi I, Yamashina S *et al.* Angiotensin type 1a receptor signaling-dependent induction of vascular endothelial growth factor in stroma is relevant to tumor-associated angiogenesis and tumor growth. *Carcinogenesis* 2005; **26**: 271–9.
13 Koh SL, Ager E, Malcontenti-Wilson C *et al.* Blockade of the renin-angiotensin system improves the early stages of liver regeneration and liver function. *J Surg Res* 2013; **179**: 66–71.
14 Childers WK. Interactions of the renin-angiotensin system in colorectal cancer and metastasis. *Int J Colorectal Dis* 2015; **30**: 749–52.
15 Ager EI, Neo J, Christophi C. The renin-angiotensin system and malignancy. *Carcinogenesis* 2008; **29**: 1675–84.
16 Wen SW, Ager EI, Neo J, Christophi C. The renin angiotensin system regulates Kupffer cells in colorectal liver metastases. *Cancer Biol Ther* 2013; **14**: 720–7.
17 Costa-Silva B, Aiello NM, Ocean AJ *et al.* Pancreatic cancer exosomes initiate pre-metastatic niche formation in the liver. *Nat Cell Biol* 2015; **17**: 816–26.
18 Sorski L, Melamed R, Matzner P *et al.* Reducing liver metastases of colon cancer in the context of extensive and minor surgeries through β-adrenoceptors blockade and COX2 inhibition. *Brain Behav Immun* 2016; **58**: 91–98.
19 Kitani H, Sakuma C, Takenouchi T *et al.* Establishment of c-myc-immortalized Kupffer cell line from a C57BL/6 mouse strain. *Results Immunol* 2014; **4**: 68–74.
20 Ogawa Y, Suzuki T, Oikawa A *et al.* Bone marrow-derived EP3-expressing stromal cells enhance tumor-associated angiogenesis and tumor growth. *Biochem Biophys Res Commun* 2009; **382**: 720–5.
21 Bataller R, Sancho-Bru P, Ginès P *et al.* Activated human hepatic stellate cells express the renin-angiotensin system and synthesize angiotensin II. *Gastroenterology* 2003; **125**: 117–25.
22 Nitou M, Ishikawa K, Shiojiri N. Immunohistochemical analysis of development of desmin-positive hepatic stellate cells in mouse liver. *J Anat* 2000; **197**: 635–46.
23 Takeda A, Stoeltzing O, Ahmad SA *et al.* Role of angiogenesis in the development and growth of liver metastasis. *Ann Surg Oncol* 2002; **9**: 610–6.
24 Sanford DE, Belt BA, Panni RZ *et al.* Inflammatory monocyte mobilization decreases patient survival in pancreatic cancer: a role for targeting the CCL2/CCR2 axis. *Clin Cancer Res* 2013; **19**: 3404–15.
25 Higashi N, Ishii H, Fujiwara T *et al.* Redistribution of fibroblasts and macrophages as micrometastases develop into established liver metastases. *Clin Exp Metastasis* 2002; **19**: 631–8.
26 Teng Y, Mu J, Hu X *et al.* Grapefruit-derived nanovectors deliver miR-18a for treatment of liver metastasis of colon cancer by induction of M1 macrophages. *Oncotarget* 2016; **7**: 25683–97.
27 Decaris ML, Emson CL, Li K *et al.* Turnover rates of hepatic collagen and circulating collagen-associated proteins in humans with chronic liver disease. *PLoS One* 2015; **10**: e0123311.
28 Yang MC, Wang CJ, Liao PC *et al.* Hepatic stellate cells secretes type I collagen to trigger epithelial mesenchymal transition of hepatoma cells. *Am J Cancer Res* 2014; **4**: 751–63. eCollection 2014.
29 Sasaki K, Murohara T, Ikeda H *et al.* Evidence for the importance of angiotensin II type 1a receptor in ischemia-induced angiogenesis. *J Clin Invest* 2002; **109**: 603–11.
30 Fujimito Y, Sasaki T, Tsuchida A *et al.* Angiotensin II type 1 receptor expression in human pancreatic cancer and growth inhibition by angiotensin II type 1 receptor antagonist. *FEBS Lett* 2001; **495**: 197–200.
31 Vinson GP, Barker S, Puddefoot JR. The renin-angiotensin system in the breast and breast cancer. *Endocr Relat Cancer* 2012; **19**: R1–19.
32 Arrieta O, Villarreal-Garza C, Vizcaíno G *et al.* Association between AT1 and AT2 angiotensin II receptor expression with cell proliferation and angiogenesis in operable breast cancer. *Tumour Biol* 2015; **36**: 5627–34.
33 Morris ZS, Saha S, Magnuson WJ *et al.* Increased tumor response to neoadjuvant therapy among rectal cancer patients taking angiotensin-converting enzyme inhibitors or angiotensin receptor blockers. *Cancer* 2016; **122**: 2487–95.
34 Neo JH, Malcontenti-Wilson C, Muralidharan V. Effect of ACE inhibitors and angiotensin II receptor antagonists in a mouse model of colorectal cancer liver metastases. *J Gastroenterol Hepatol* 2007; **22**: 577–84.
35 Krüger A. Premetastatic niche formation in the liver: emerging mechanisms and mouse models. *J Mol Med (Berl)* 2015; **93**: 1193–201.

36 Gordon KJ, Blobe GC. Role of transforming growth factor-beta superfamily signaling pathways in human disease. *Biochim Biophys Acta* 2008; **1782**: 197–228.
37 Moustakas A, Heldin GH. Mechanism of TGF-b-induced epithelial-mesenchymal transition. *J Clin Med* 2016;**5**: pii: E63. https://doi.org/10.3390/jcm5070063.
38 Carvajal G1, Rodríguez-Vita J, Rodrigues-Díez R *et al.* Angiotensin II activates the Smad pathway during epithelial mesenchymal transdifferentiation. *Kidney Int* 2008; **74**: 585–95.
39 Noy R, Pollard JW. Tumor-associated macrophages: from mechanisms to therapy. *Immunity* 2014; **41**: 49–61.
40 Niedzwiecki A, Roomi MW, Kalinovsky T *et al.* Micronutrient synergy–a new tool in effective control of metastasis and other key mechanisms of cancer. *Cancer Metastasis Rev* 2010; **29**: 529–42.
41 Wen SE, Ager EI, Christophi C. Biomodal roleof Kupffer cells during colorectal cancer liver metastasis. *Cancer Biol Ther* 2013; **14**: 606–13.
42 Kruse J, von Bernstorff W, Evert K *et al.* Macrophages promote tumour growth and liver metastasis in an orthotopic syngeneic mouse model of colon cancer. *Int J Colorectal Dis* 2013; **28**: 1337–49.
43 Okamoto K, Tajima H, Nakanuma S *et al.* Angiotensin II enhances epithelial-to-mesenchymal transition through the interaction between activated hepatic stellate cells and the stromal cell-derived factor-1/CXCR4 axis in intrahepatic cholangiocarcinoma. *Int J Oncol* 2012; **41**: 573–82.

Supporting Information

Additional Supporting Information may be found online in the supporting information tab for this article:

Fig. S1. Effect of AT1a signaling on liver metastasis formation after injection of Colon 38 cells. (a) Typical growth appearance of liver metastasis in WT and AT1aKO mice injected intrasplenically with Colon 38 cells. Arrows indicate metastatic colonization. Scale bar = 1 cm. (b) Effect of AT1a signaling on liver metastasis formation 2 weeks after injection of Colon 38 cells. Data are presented as the means ± SD of six mice per group. $P < 0.05$ *versus* WT.

Fig. S2. Representative images of double immunofluorescence staining of AT1a and F4/80 or desmin in metastatic livers from WT mice. Double immunofluorescence staining of AT1a (green) and F4/80 (red) (a) or desmin (red) (b) in metastatic liver of WT at 14 days after CMT-93 injection. T, tumor. Scale bar = 100 μm.

Fig. S3. Representative images showing immunofluorescence staining of type I collagen and desmin or F4/80 in metastatic livers from WT mice. Double immunofluorescence staining of type I collagen (green) and desmin (red) (a) or F4/80 (red) (b) in metastatic livers of WT mice at 14 days after CMT-93 injection. Expression of type I collagen was colocalized with desmin$^+$ cells, but not F4/80$^+$ cells in metastatic areas. Arrow heads indicate double-positive cells. T, tumor. Scale bar = 100 μm.